Dynamic control of photoluminescence polarization properties in GaAs/AlAs quantum wells by surface acoustic waves

Tetsuomi Sogawa,[1,*] Haruki Sanada,[1] Hideki Gotoh,[1] Hiroshi Yamaguchi,[1] and Paulo V. Santos[2]
[1]*NTT Basic Research Laboratories, NTT Corporation, 3-1 Morinosato-Wakamiya, Atsugi, Kanagawa 243-0198, Japan*
[2]*Paul Drude Institute, Hausvogteiplatz 5-7, 10117 Berlin, Germany*
(Received 29 March 2012; published 13 July 2012)

We have investigated the dynamic polarization properties of photoluminescence (PL) spectra in GaAs/AlAs quantum wells (QWs) modulated by surface acoustic waves (SAWs) in various configurations. One-dimensional standing SAWs, which are formed by the interference of two counterpropagating SAW beams, exhibit emission energy oscillations due to strain-induced band gap modulation. When the band gap energy reaches its minimum value, the PL spectra exhibit the strongest polarization anisotropy, with preferential emission along the direction perpendicular to SAW propagation. Two-dimensional SAWs formed by the interference between two orthogonally propagating SAW beams also cause the emission energy to oscillate, while no polarization anisotropy appears. In contrast, a $\pi/2$ relative phase difference, which is electrically introduced between the two SAWs, significantly alters both the PL spectra and the polarization anisotropy. The oscillation of the emission energies disappears and the polarized direction changes every quarter SAW period. These SAW phase-dependent changes in the polarization properties are explained by considering the exciton motion under the quadrupolelike SAW modulation, which is formed by the two orthogonal unbalanced standing SAWs with a phase difference of $\pi/2$.

DOI: 10.1103/PhysRevB.86.035311 PACS number(s): 77.65.Dq, 78.55.−m, 78.47.jd, 78.67.−n

I. INTRODUCTION

Among a variety of attempts to improve or modify the electric and optical properties of materials, the introduction of the quantum confinement in artificial semiconductor structures such as quantum-well (QW) structures has been one of the most successful ways which contribute to fundamental scientific studies and actual device applications.[1] One-dimensional (1D) and zero-dimensional (0D) quantum confinement structures have also been intensively studied by many research groups for the further improvement of the device performance as well as for discovering novel physical phenomena. The strong polarization anisotropy of the interband transitions in quantum wires (QWRs) induced by 1D quantum confinement has attracted a lot of attention for device applications in photonic network systems. It has been reported that the polarization anisotropy can be controlled by changing the cross-sectional shapes of the QWRs, where the relative strength between lateral and vertical confinements significantly modifies the mixing states between the heavy-hole band (HH) and the light-hole band (LH).[2] In such statically controlled quantum structures, the polarization anisotropy and the optical transition energies are determined by the structures. In contrast, surface acoustic wave (SAW) technology combined with the QWs is known to provide 1D and 0D dynamically confined structures called dynamic quantum wires and dynamic quantum dots (DQDs), respectively.[3–13] The SAWs are generated by applying radio frequency (rf) electrical signals to interdigital transducers (IDTs) formed on a piezoelectric sample such as GaAs/AlAs QWs.[7–10] Such dynamically confined structures have the advantage that quantum confinement created by the laterally modulated piezoelectric potential (Φ_{SAW}) can be controlled electrically and that the spatial period of the lateral modulation of Φ_{SAW} is uniform. In addition, dynamic polarization anisotropies, defined as temporally and spatially varying polarization properties controlled by external electrical signals, have been demonstrated.[3–6] Furthermore, these dynamically confined structures enable the long-distance electron spin transport and coherent spin manipulation.[14–17]

In this paper we investigate the dynamic polarization anisotropy of the photoluminescence (PL) spectra in GaAs/AlAs QWs under various SAW configurations by using a microscopic PL setup. The first configuration was 1D-standing SAWs, which were formed by the interference between two counterpropagating SAW beams. We found a periodic emission energy oscillation due to the strain-induced band gap modulation. Time-resolved polarization anisotropy spectra obtained under the 1D-standing SAWs reveal that the PL polarization anisotropy becomes the strongest when the band gap energy reaches its minimum value and that the preferentially polarized direction is perpendicular to the SAW propagating direction. Then, we investigated the PL properties under the two-dimensional (2D) SAW, where the interference between two orthogonally propagating SAW beams forms the DQDs. Previous studies established that the 2D SAW forms two kinds of interpenetrating square arrays of DQDs, that is, one is called as potential dynamic dots (p-DDs), which are created by the modulation of Φ_{SAW}, and the other as strain dynamic dots (s-DDs), which are formed by the strain-induced band gap modulation.[5,11] It was also demonstrated that PL polarization anisotropy takes place at only the p-DDs.[5] In the present experiment we found that the time-resolved PL spectra from the DQDs exhibit emission energy oscillations similar to the results for the 1D-standing SAWs, while no polarization anisotropy appears. In contrast, if a relative phase difference of $\pi/2$ is introduced between the two SAWs, the band gap oscillation disappears and, in turn, the PL polarization periodically changes direction. This polarization oscillation is attributed to the exciton migration driven by the quadrupolelike SAW modulation of the band structures. A theoretical analysis of the band structure and optical transition properties under the quadrupolelike SAW modulation qualitatively explains the experimental results.

In Sec. II we describe the sample structures and experimental techniques used to measure the PL spectra and polarization dynamics under acoustic excitation. In Sec. III we present the experimental results of the time-resolved PL and anisotropy spectra modulated by the 1D-standing SAWs (Sec. III A) and by the 2D-traveling SAWs (Sec. III B). Then we theoretically analyze the modulation of the band structures and PL anisotropy for the quadrupolelike SAWs to explain the experimental results (Sec. IV). Our conclusions are summarized in Sec. V.

II. EXPERIMENTAL DETAILS

Low temperature (4 K) spatially and time-resolved PL spectra were measured in a helium gas-flow cryostat using a confocal micro-PL setup with a 45 × objective lens. The measurements were performed on a sample containing eight GaAs single QWs with various well thicknesses L_z (= 6.3, 7.1, 8.3, 9.9, 12.2, 15.2, 19.8, and 83 nm) separated by seven-period AlAs(2.0 nm)/GaAs(2.0 nm) short-period superlattice barriers grown on (001) GaAs by molecular beam epitaxy. The QWs were located between 100 and 400 nm from the surface. Four IDTs were deposited in a cruciform arrangement to generate SAWs propagating along the [110] and [1−10] directions, as illustrated in Fig. 1(a), where the IDTs are labeled A–D and the horizontal ([010]) and vertical ([−100]) axes are denoted by X and Y, respectively. The sample is rotated by 45 deg to compensate the residual polarization properties of the optical setup, where $PL_{[1-10]}$ (red arrow) and $PL_{[110]}$ (blue arrow) represent the PL components polarized parallel to the [1−10] and [110] direction, respectively. As the SAW frequency (f_{SAW}) is 820 MHz, that is, the SAW period (T_{SAW}) is 1.2 ns, the SAW wavelength (λ_{SAW}) corresponds to approximately 3.6 μm, as obtained from the SAW phase velocity (v_{SAW}) of 2950 m/s. Mode-locked pulses (1.5 ps, 82 MHz, 720 nm) from a Ti-sapphire laser synchronized with the SAW frequency were used to generate carriers, that is, one optical excitation pulse for every 10 T_{SAW}. The PL was spectrally analyzed by using a spectrometer connected to a synchronously scanning streak camera with a time resolution of 10 ps or to a charge-coupled device (CCD) detector. The SAW linear power density P_l per beam was roughly estimated to range from 70 to 100 W/m by comparing the observed band gap energy shifts in the PL spectra and the theoretical values, where P_l is defined as the acoustic power flux per unit length along the cross section of the SAW beam.[3] In this study we define the PL intensity (PL_{sum}), the PL difference (PL_{dif}), and the degree of polarization anisotropy (ρ) as ($PL_{[1-10]} + PL_{[110]}$), ($PL_{[1-10]} - PL_{[110]}$), and ($PL_{[1-10]} - PL_{[110]}$)/($PL_{[1-10]} + PL_{[110]}$), respectively.

Figures 1(b) and 1(c) are schematic illustrations of the in-plane components of the lattice displacement field under a 1D SAW (in the [1−10] direction) and a 2D SAW (in the [110] and [1−10] directions), respectively. The 1D SAW causes spatial modulation of the band gap energy due to the strain. The compressive (tensile) strain results in 1D arrays with

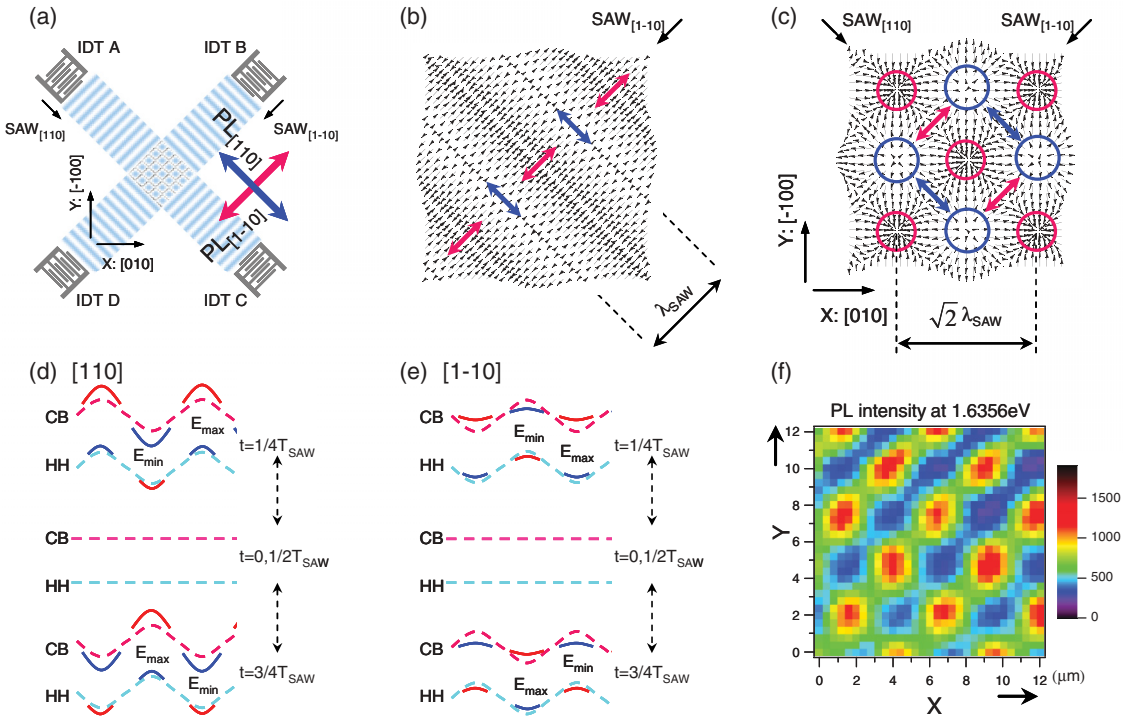

FIG. 1. (Color) (a) Sample layout with four IDTs (IDT A–D) deposited in a cruciform arrangement to generate SAWs propagating along the [110] and [1−10] directions. (b) Schematic illustration of the in-plane components of the particle displacement field under a 1D SAW (along [1−10]), and (c) under a 2D SAW (along [110] and [1−10]). (d) Band modulation by the 1D-standing SAW along the [110] direction, and (e) along the [1−10] direction. The dashed lines display the modulation of the electronic energy ($-q\Phi_{SAW}$) for CB and HH, while the solid lines represent the strain-induced energy shifts of the CB and HH (not to scale). (f) A typical PL intensity mapping result under the traveling 2D SAW for a 6.3-nm QW. Here the PL was recorded in the higher-energy side of the PL peak to display the s-DDs.

enhanced (reduced) band gap energy, where the preferential polarization is parallel (perpendicular) to the SAW direction, as represented by red (blue) arrows in Fig. 1(b). Although the preferential polarization direction depends on the depth normalized by λ_{SAW},[6] the QWs used in this experiment show the above relation between the strain and the polarization. The interference of counterpropagating SAW beams of equal amplitude forms a 1D-standing SAW, which causes the band modulation to oscillate between the 1D and 2D states,[13] as shown in Figs. 1(d) and 1(e) for the SAWs along [110] and [1−10], respectively. The dashed lines show the modulation of the electronic energy ($-q\Phi_{SAW}$) for the conduction band (CB) and HH. The solid lines, which are exaggerated compared with the scale for the dashed lines, represent the strain-induced energy shifts of the CB and HH. For the normalized depth of the QWs, the band modulation is of type II, that is, both the CB and HH shift toward the same direction.[6] E_{max} (E_{min}) denotes the antinode positions where the band gap energy is at its maximum (minimum) value owing to the compressive (tensile) SAW strain. At the antinode positions the band gap energy oscillates between E_{max} and E_{min} with a period of T_{SAW}, and thus the flat-band condition, that is, the 2D state, appears every $T_{SAW}/2$. At the node positions, in contrast, the band gap energy does not change but the lateral piezoelectric field and the lateral effective field driving the exciton migration vary every $T_{SAW}/2$.

It is known that the D_{4d} symmetry of the GaAs lattice causes the sign of Φ_{SAW} to be opposite for SAWs along the [110] and [1−10] directions,[6,18] as shown in Figs. 1(d) and 1(e). As a result, the Φ_{SAW} modulation disappears at the location of the compressive (tensile) s-DDs, that is, E_{max} (E_{min}) sites, denoted by red (blue) circles in Fig. 1(c).[5] It should be mentioned that these s-DDs exhibit no polarization anisotropy because of the isotropic in-plane strain. On the other hand, p-DDs located at the saddle points of the band gap modulation exhibit polarization anisotropy, where the preferential polarization directions are indicated by red or blue arrows. Figure 1(f) shows a typical result for the PL intensity mapping (12 × 12 μm) under the 2D-traveling SAW for the 6.3 nm QW detected by the CCD. As the IDTs A and B were used to form a square array of DQDs, the DQDs are moving in the −Y direction (i.e., towards the bottom) with a velocity of $\sqrt{2}v_{SAW}$. Since the PL mapping is recorded at a photon energy of 1.6356 eV, which is higher than the PL peak of 1.630 eV as observed in the absence of a SAW, the strong PL sites in Fig. 1(f) correspond to the compressive s-DDs. The detailed characteristics of the DQDs are described in Ref. 5. For the mapping measurement we used a laser power density of 500 W/cm^2 and set a window size of a variable cross slit located at the confocal point less than 200 × 200 μm to obtain a spatial resolution of approximately 1 μm.

III. RESULTS

A. Time-resolved and anisotropic PL spectra under 1D-standing SAWs

Figures 2(a)–2(c) show time-resolved PL_{sum}, PL_{dif}, and ρ spectra in the absence of a SAW for the laser power density of 500 W/cm^2, where scale-out data are shown in white. The PL_{sum} spectra exhibit the typical monotonous decay of excitonic recombination in QWs. Figure 2(c) shows zero ρ signals around the center energies of each emission peak, which are referred to as "flat-band energies" in this report and indicated by dashed white or black lines in each figure. The PL_{sum}, PL_{dif}, and ρ spectra under the 1D-standing SAWs along the [110] direction are shown in Figs. 2(d)–2(f), respectively, where rf power was applied to IDTs A and C. We increased the laser power density to 1500 W/cm^2 and the window size of the cross slit to 400 × 400 μm to improve the signal to noise ratio of the ρ spectra. Since lateral piezoelectric fields are strongly screened by the photoexcited carriers under this relatively intense excitation condition, the PL quenching due to the exciton ionization becomes less effective than in previous reports that used a weaker excitation condition.[5,6,19] Thus the PL spectra are mainly determined by the spatial dynamics of excitons driven by the band gap gradient. As the carriers were generated when the band modulation was flat [i.e., $t = 0$ or $1/2\ T_{SAW}$ in Fig. 1(d)], the emissions start from the flat-band energies denoted by the dashed white lines, and progressively decrease to the minimum energies that correspond to E_{min} around $t = 300$ ps, as shown in Fig. 2(d). Then, the emission energies return to the flat-band energies and decrease again. The modulation is repeated every half T_{SAW} of 600 ps. Figures 2(g)–2(i) show results obtained under the 1D-standing SAWs along [1−10], where the phases of the SAWs from IDTs B and D were electrically tuned so that the emission energies start from E_{min} and then reach the flat-band energies around $t = 300$ ps. Figures 2(f) and 2(i), where the red (blue) signals correspond to polarization parallel to the [1−10] ([110]) direction, demonstrate that the PL anisotropy becomes the strongest when the band gap is minimum and that the preferential polarization is perpendicular to the SAW direction. The reason why the values of $|\rho|$ observed around E_{min} are larger than those around E_{max} is that the mixing between the HH and LH states is stronger for the E_{min} sites, as was theoretically analyzed in Ref. 1.

If we selectively detect the PL signal from only one antinode, the oscillatory behavior of the emission energies should be as follows: (i) the emission energies simply oscillate between E_{min} and E_{max} when the excitons have extremely low mobility, or (ii) the emissions appear between E_{min} and the flat-band energies and disappear while the band gap is larger than the flat-band values due to the escape of excitons from the detection spot with relatively high mobility.[13] In both cases the emissions around E_{min} should appear every T_{SAW}, inconsistent with the experimental finding that the emission energies oscillate at $2f_{SAW}$ between the E_{min} and flat-band energies. By considering the poorer spatial resolution compared with the measurement in Fig. 1(b) due to the use of the larger cross-slit window, the emission energy oscillation at $2f_{SAW}$ is attributed to the simultaneous detection of the emissions from more than two adjacent antinodes, which are separated by $\lambda_{SAW}/2$ of 1.8 μm. As another evidence of the simultaneous signal detection from the separated antinodes, we detected emissions from excitons staying around the E_{max} sites besides emissions from the E_{min} sites, as observed in the PL_{dif} spectra [see Figs. 2(e) and 2(h)]. These higher-energy side emissions with opposite preferential polarization compared to the lower-energy ones are clearly observed when

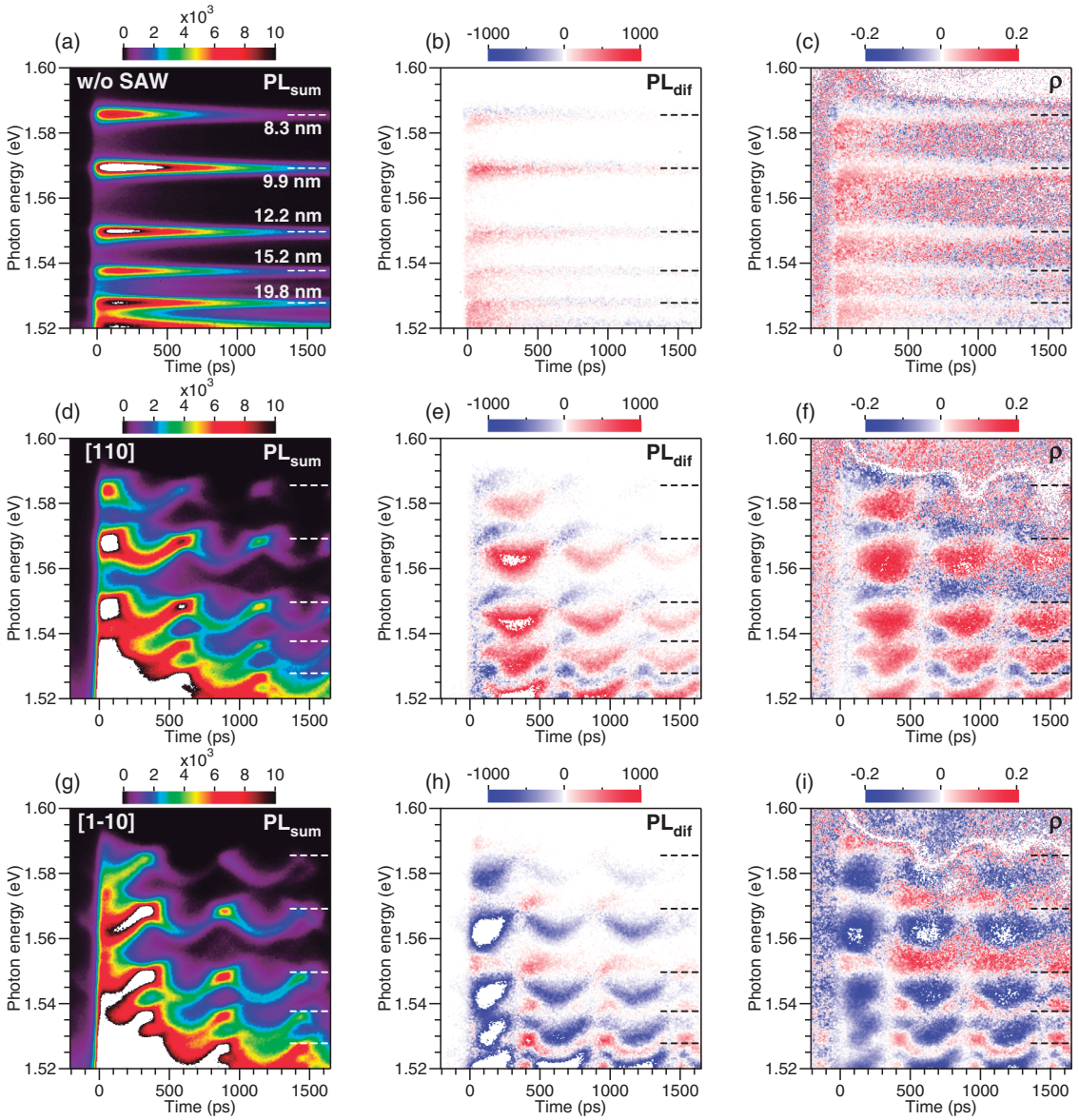

FIG. 2. (Color) (a)–(c) Time-resolved PL_{sum}, PL_{dif}, and ρ spectra in the absence of a SAW, respectively. Corresponding spectra for a 1D-standing SAW along the [(d)–(f)] [110] direction and [(g)–(i)] [1−10] direction.

the band gap begins to increase from the flat-band energies indicated by dashed black lines, while they become weaker after the band gap reaches its maximum value due to the escape of the excitons into the lower-energy sites.

B. Oscillation of polarization anisotropy controlled by phases of 2D SAWs

Figures 3(a)–3(c) show the PL_{sum}, PL_{dif}, and ρ spectra, respectively, under the 2D-traveling SAW with SAW phases for IDTs A and B of $(\theta_A, \theta_B) = (0, 0)$, where (0, 0) corresponds to the phases that form an array of moving DQDs as observed in Fig. 1(f). We adopted the same excitation laser power P_l for each SAW beam, and the measurement setup that we used in the 1D-standing SAW experiment. Figure 3(a) shows that the emission energies oscillate at $2f_{SAW}$ between E_{min} and the flat-band energies. This suggests that excitons do not come close to the arriving E_{max} sites but move diagonally, that is, in the [−1−10] or [−110] direction along the blue or red arrows of Fig. 1(c), from initially trapped E_{min} sites to the nearest E_{min} sites during a half T_{SAW}. In addition to the absence of anisotropic emission from the E_{min} sites, which correspond to the tensile s-DD, excitons emitting around the flat-band energies also exhibit no anisotropy, as shown in Figs. 3(b) and 3(c), although the p-DDs must have a strong anisotropy.[5] Since the emissions from two side-by-side p-DDs with opposite anisotropy are detected simultaneously, the PL signals totally cancel the anisotropy. In this way the excitons moving along the zigzag paths exhibit no anisotropy.

We found that the energetic oscillatory behavior disappears by electrically adding a $\pi/2$ phase difference only to IDT B, as shown in Fig. 3(d). Interestingly, Figs. 3(e) and 3(f) demonstrate that the polarization direction changes every quarter T_{SAW} of 300 ps. We also found that the initial

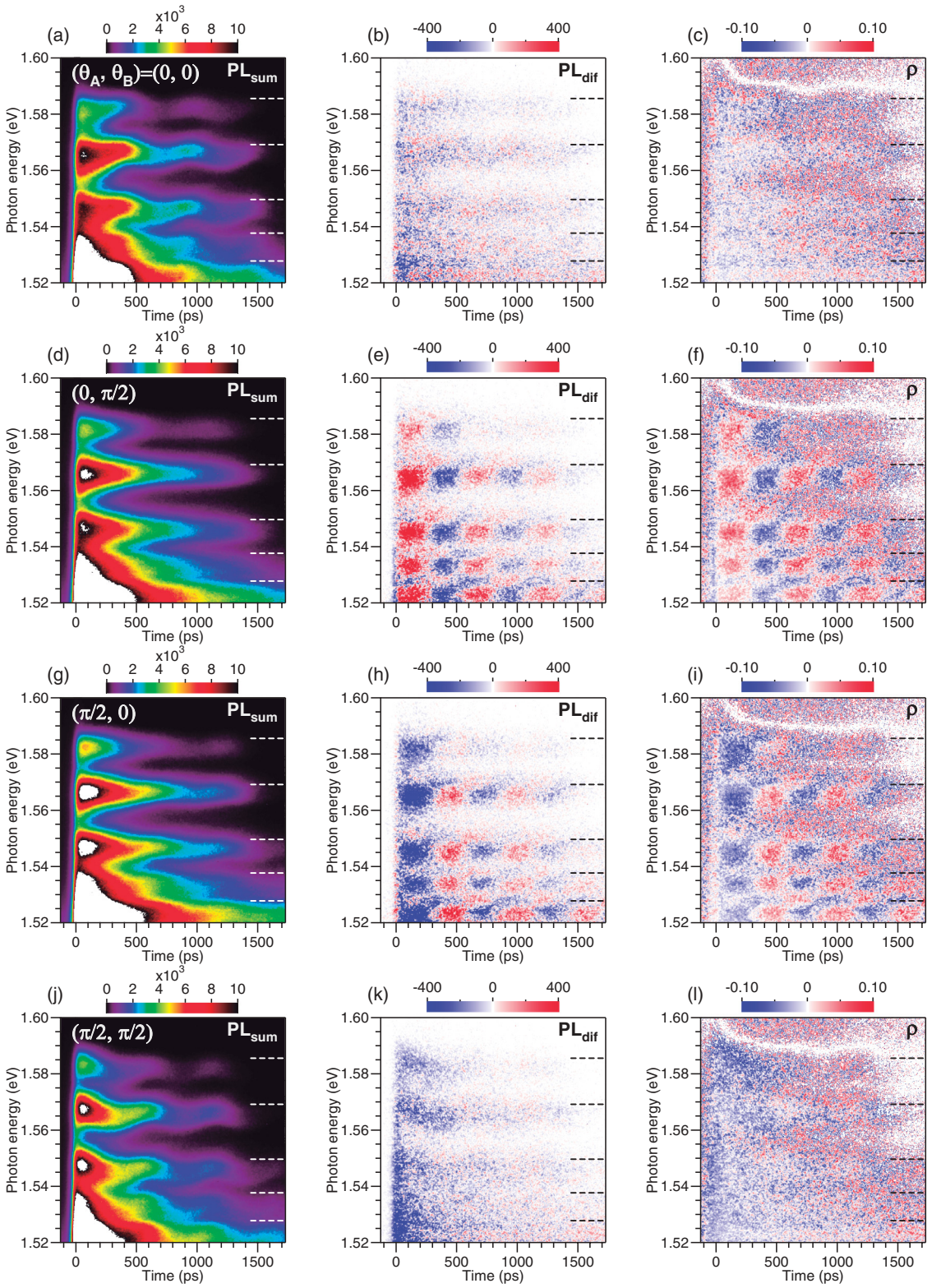

FIG. 3. (Color) (a)–(c) Time-resolved PL_{sum}, PL_{dif}, and ρ spectra, respectively, under the 2D SAW for phases of $(\theta_A, \theta_B) = (0, 0)$, (d)–(f) for $(0, \pi/2)$, (g)–(i) for $(\pi/2, 0)$, and (j)–(l) for $(\pi/2, \pi/2)$.

polarization direction is altered by adding the $\pi/2$ phase difference only to IDT A, as shown in Figs. 3(h) and 3(i). If we give a $\pi/2$ phase difference to both IDTs, the emission energy oscillation is reproduced and the anisotropy oscillation disappears, as shown in Figs. 3(j)–3(l). Since Figs. 3(a) and 3(j) show that the PL emissions start from the E_{min} energies and flat-band energies, respectively, the phases of $(\pi/2, \pi/2)$ cause a time shift by a quarter T_{SAW}.

IV. DISCUSSION

Since the combination of the time-resolved measurement and the 1D-standing SAW technique under the high carrier density condition provides stable observation of the PL modulation, we obtained more easily interpreted data for the dynamic PL anisotropy compared to the synchronized measurement for 1D-traveling SAW using a CCD.[6] The emission energy oscillation observed under the 2D-traveling SAW can be explained by the characteristics of the DQDs.[5] In contrast, neither the oscillation of the PL anisotropy at $2f_{\mathrm{SAW}}$ nor the disappearance of the emission energy oscillation induced by the $\pi/2$ phase difference can be explained by the DQDs formed by the 2D SAW modulation. Since the introduction of the $\pi/2$ phase difference between the orthogonal SAW beams is essential in causing the phenomena, we will explain the results by analogy with a quadrupole oscillation. If a perfect quadrupole modulation is obtained by using orthogonal two pairs of well-balanced standing SAWs with a $\pi/2$ relative phase difference between the pairs, the dimensionality of the modulation oscillates between 0D and 1D and the direction of the 1D modulation turns by 90 deg every quarter T_{SAW}. In the present experimental situation, unbalanced standing waves are likely to be formed due to the partial reflection of the SAW beams at the opposite ITDs or cleaved edges of the sample. In general, one unbalanced standing wave produces moving antinodelike positions, and the amplitude around the antinodelike positions oscillates at $2f_{\mathrm{SAW}}$. Two orthogonal unbalanced standing SAWs should form an imperfect quadrupole modulation if the relative phase is tuned to $\pi/2$, while an array of moving DQDs with oscillating modulation amplitude is formed for the case of no phase difference.

Figures 4(a)–4(h) show the calculated results on the spatial modulation of the strain-induced shift of the CB-HH transition energy under quadrupolelike SAW fields plotted for every 1/8 T_{SAW} interval, where the X and Y scales are normalized by the lattice constant of the DQD array $\lambda^{*}_{\mathrm{SAW}}$ ($=\sqrt{2}\lambda_{\mathrm{SAW}}$). The framework of the theoretical calculation is described in Ref. 3. We performed the calculations for a QW with a HH-LH energy splitting of 20 meV and located 175 nm below the surface using an f_{SAW} of 800 MHz and a P_l of 100 W/m per SAW beam. In this calculation we consider the partial reflection of the SAW power (amplitude) of 6.25% (25%) and neglect multiple reflection effects. Note that a 1D-like elongated modulation and a 2D modulation appear alternately every 1/8 T_{SAW}. Assume that the excitons are generated at $t = 0$ within the excitation and detection spot centered at (X, Y) = (0.8, 1.3), as indicated by a dashed black circle in Fig. 4(a). The excitons quickly migrate to the nearest E_{min} position denoted by "+" under the condition that the band gap modulation dominates the exciton motion because of the screening of Φ_{SAW}. White arrows schematically represent the exciton motion toward the E_{min} sites. When the band modulation becomes 1D-like again at $t = 2/8\ T_{\mathrm{SAW}}$, the barrier height separating the nearest E_{min} sites is reduced by approximately 2 meV compared with that of 5 meV for the 2D modulation at $t = 1/8\ T_{\mathrm{SAW}}$. Thus, a part of the excitons moves from the initially trapped E_{min} sites to the next arriving E_{min} sites along the 1D-like modulation, as indicated by the longer arrow in Fig. 4(c). Then, 1D-like modulation is repeated every quarter T_{SAW}, resulting in the spatial broadening of the excitons attracted toward the E_{min} sites. If no phase difference is introduced between the two SAWs, the square array of the DQDs as observed at $t = 1/8$, $3/8$, $5/8$, and $7/8\ T_{\mathrm{SAW}}$ moves toward the bottom

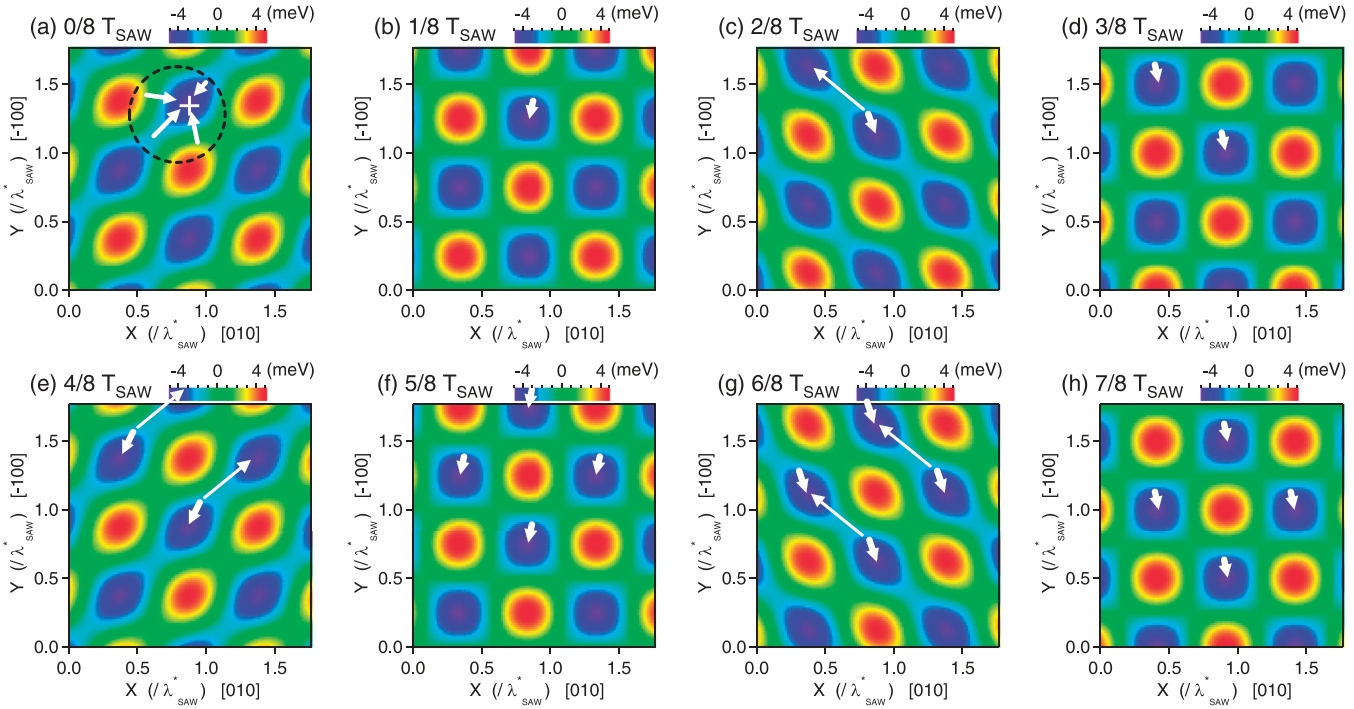

FIG. 4. (Color) (a)–(h) Calculated results on the spatial modulation of the strain-induced shift of the CB-HH transition energy under the quadrupolelike SAW modulation, plotted for every 1/8 T_{SAW} interval.

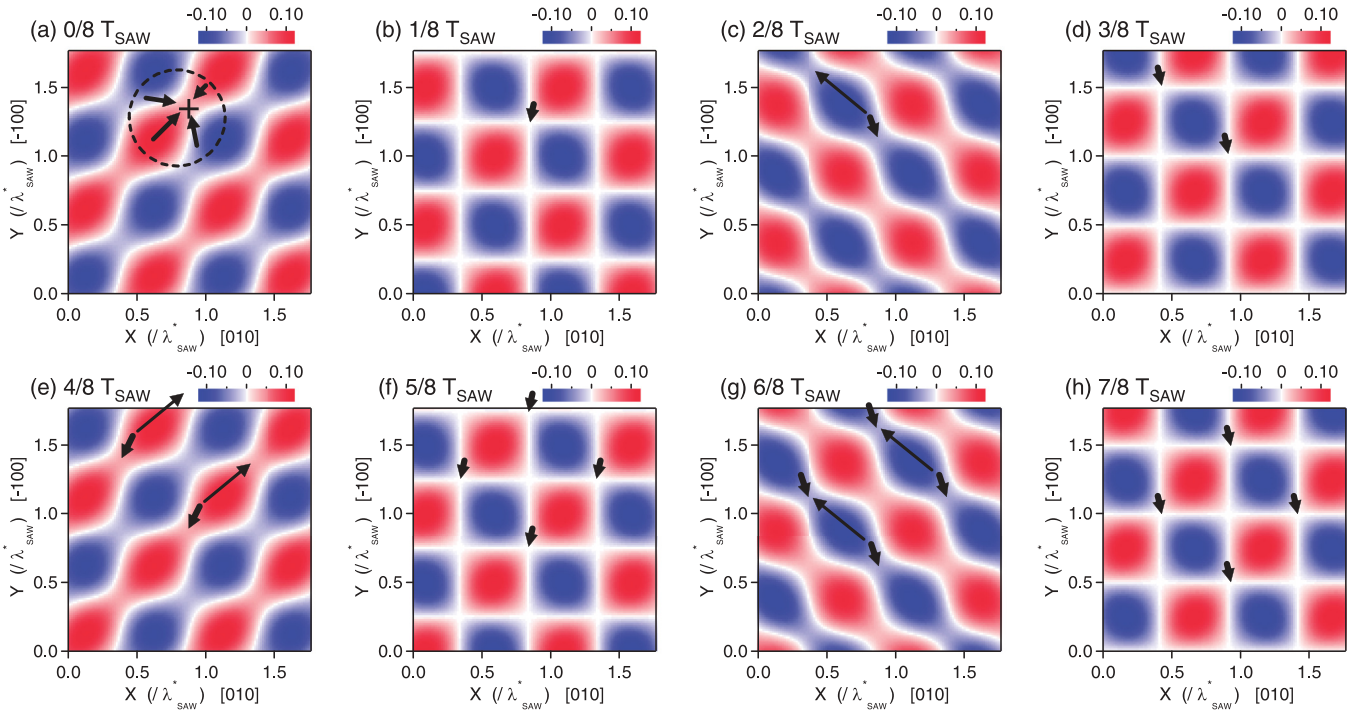

FIG. 5. (Color) (a)–(h) Calculated results on the spatial modulation of ρ for the CB-HH transition under the quadrupolelike SAW, plotted for every $1/8\ T_{\mathrm{SAW}}$ interval.

while maintaining the symmetric shape of the DQDs. The energetic oscillations between E_{min} and the flat-band energies as observed in Figs. 3(a) and 3(d) suggest that some part of the excitons moves diagonally from one E_{min} site to the nearest E_{min} site across the p-DD areas with a barrier height of several meV when the next E_{max} site, that is, compressive s-DD, comes close, while the remaining excitons move toward the bottom together with the initially trapped E_{min} site.

Figures 5(a)–5(h) show the calculated results on the corresponding spatial modulation of ρ, where black arrows represent the exciton motion at the same positions as in Fig. 4. By considering the experimental results that the emission energies are lower than the flat-band energies [see Figs. 3(d) and 3(g)], most of the excitons should emit near the E_{min} sites as denoted by the arrowheads. When the 2D modulation is formed at $t = 1/8$, $3/8$, $5/8$, and $7/8\ T_{\mathrm{SAW}}$, the center of the E_{min} sites exhibits no anisotropy because of the isotropic in-plane strain. When the modulation becomes 1D-like at $t = 0/8$, $2/8$, $4/8$, and $6/8\ T_{\mathrm{SAW}}$, ρ has nonzero values even at the center of the E_{min} sites. Note that the polarization direction under the 1D-like modulation turns every quarter T_{SAW} [see Figs. 5(a), 5(c), 5(e), and 5(g)]. We also confirmed that the initial polarization is switched by changing the phase combination (not shown here). Therefore, the calculated results for the temporal behaviors of the anisotropy are in good agreement with the experimental findings.

V. CONCLUSIONS

We have investigated the dynamic polarization properties of PL spectra controlled by SAWs in GaAs/AlAs QWs. 1D-standing SAWs, which are formed by the interference between two counterpropagating SAW beams, cause a periodic modulation of emission energies due to the strain-induced band gap modulation. Time-resolved measurements demonstrated that the strongest PL polarization anisotropy appears and the polarized direction is perpendicular to the SAW propagating direction when the band gap energy reaches its minimum. DQDs formed by the 2D SAWs, that is, by the interference between two orthogonally propagating SAW beams, also exhibit emission energy oscillation, while no anisotropy appears. In contrast, by introducing a relative phase difference of $\pi/2$ electrically between the two SAWs, we found that the sign of the polarization anisotropy changes every quarter T_{SAW} of 300 ps. This polarization oscillation is explained by considering the exciton motion driven by the quadrupolelike modulation of the band structures. The modulation is produced by the interference between the two pairs of orthogonal unbalanced standing SAWs, one of which is delayed by $\pi/2$. A theoretical analysis on the band structures and optical transition properties modulated by the quadrupolelike SAW configuration consistently explains the experimental results. These findings in this study are expected to provide novel photonic devices based on electrically controlled optical polarization anisotropy induced by SAWs in QWs that have intrinsically no in-plane polarization anisotropy.

ACKNOWLEDGMENTS

We gratefully acknowledge T. Tawara and S. Miyashita for fruitful discussions, comments, and a supply of high-quality samples. This work was partly supported by Grant-in-Aid for Scientific Research from the Japan Society for the Promotion of Science (19310067, 23310097).

*sogawa.tetsuomi@lab.ntt.co.jp

[1]C. Weisbuch and B. Vinter, *Quantum Semiconductor Structures, Fundamentals and Applications* (Academic, San Diego, CA, 1991).
[2]T. Sogawa, H. Ando, S. Ando, and H. Kanbe, Phys. Rev. B **56**, 1958 (1997).
[3]T. Sogawa, P. V. Santos, S. K. Zhang, S. Eshlaghi, A. D. Wieck, and K. H. Ploog, Phys. Rev. B **63**, 121307(R) (2001).
[4]P. V. Santos, F. Alsina, J. A. H. Stotz, R. Hey, S. Eshlaghi, and A. D. Wieck, Phys. Rev. B **69**, 155318 (2004).
[5]T. Sogawa, H. Sanada, H. Gotoh, H. Yamaguchi, S. Miyashita, and P. V. Santos, Phys. Rev. B **80**, 075304 (2009).
[6]T. Sogawa, H. Sanada, H. Gotoh, H. Yamaguchi, and P. V. Santos, Appl. Phys. Lett. **100**, 162109 (2012).
[7]J. M. Shilton, V. I. Talyanskii, M. Pepper, D. A. Ritchie, J. E. F. Frost, C. J. B. Ford, C. G. Smith, and G. A. C. Jones, J. Phys.: Condens. Matter **8**, L531 (1996).
[8]C. Rocke, S. Zimmermann, A. Wixforth, J. P. Kotthaus, G. Böhm, and G. Weimann, Phys. Rev. Lett. **78**, 4099 (1997).
[9]P. V. Santos, M. Ramsteiner, and F. Jungnickel, Appl. Phys. Lett. **72**, 2099 (1998).
[10]P. V. Santos, Appl. Phys. Lett. **74**, 4002 (1999).
[11]F. Alsina, J. A. H. Stotz, R. Hey, and P. V. Santos, Solid State Commun. **129**, 453 (2004).
[12]T. Sogawa, H. Gotoh, Y. Hirayama, P. V. Santos, and K. H. Ploog, Appl. Phys. Lett. **91**, 141917 (2007).
[13]T. Sogawa, H. Sanada, H. Gotoh, H. Yamaguchi, S. Miyashita, and P. V. Santos, Appl. Phys. Lett. **94**, 131912 (2009).
[14]T. Sogawa, P. V. Santos, S. K. Zhang, S. Eshlaghi, A. D. Wieck, and K. H. Ploog, Phys. Rev. Lett. **87**, 276601 (2001).
[15]J. A. H. Stotz, R. Hey, P. V. Santos, and K. H. Ploog, Nat. Mater. **4**, 585 (2005).
[16]O. D. D. Couto, F. Iikawa, J. Rudolph, R. Hey, and P. V. Santos, Phys. Rev. Lett. **98**, 036603 (2007).
[17]H. Sanada, T. Sogawa, H. Gotoh, K. Onomitsu, M. Kohda, J. Nitta, and P. V. Santos, Phys. Rev. Lett. **106**, 216602 (2011).
[18]F. Alsina, P. V. Santos, and R. Hey, Phys. Rev. B **65**, 193301 (2002).
[19]T. Sogawa, H. Sanada, H. Gotoh, H. Yamaguchi, S. Miyashita, and P. V. Santos, Jpn. J. Appl. Phys., Part 2 **46**, L758 (2007).